Current Biology, Volume *27*

Supplemental Information

Unmasking Transcriptional Heterogeneity in Senescent Cells

Alejandra Hernandez-Segura, Tristan V. de Jong, Simon Melov, Victor Guryev, Judith Campisi, and Marco Demaria

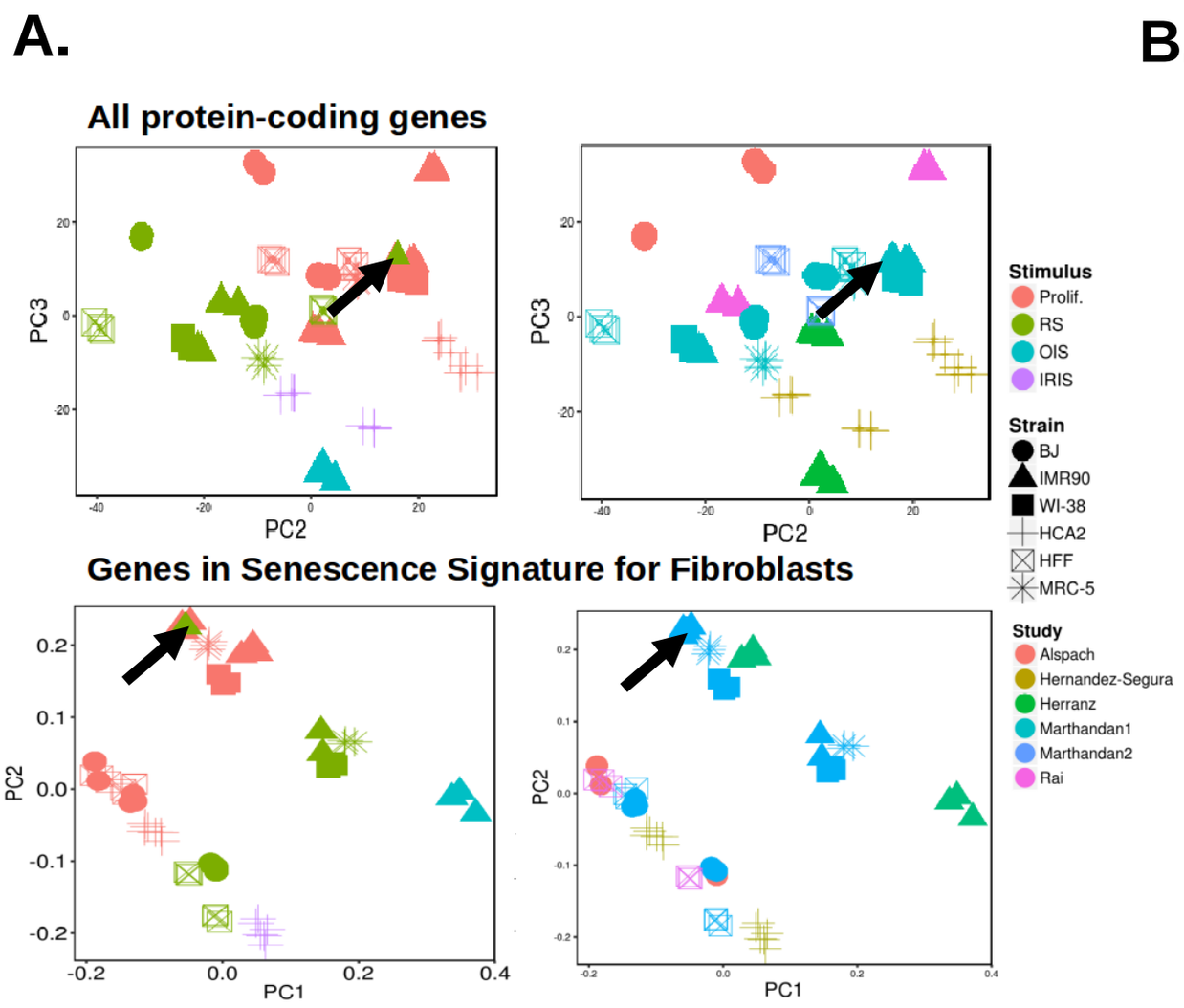

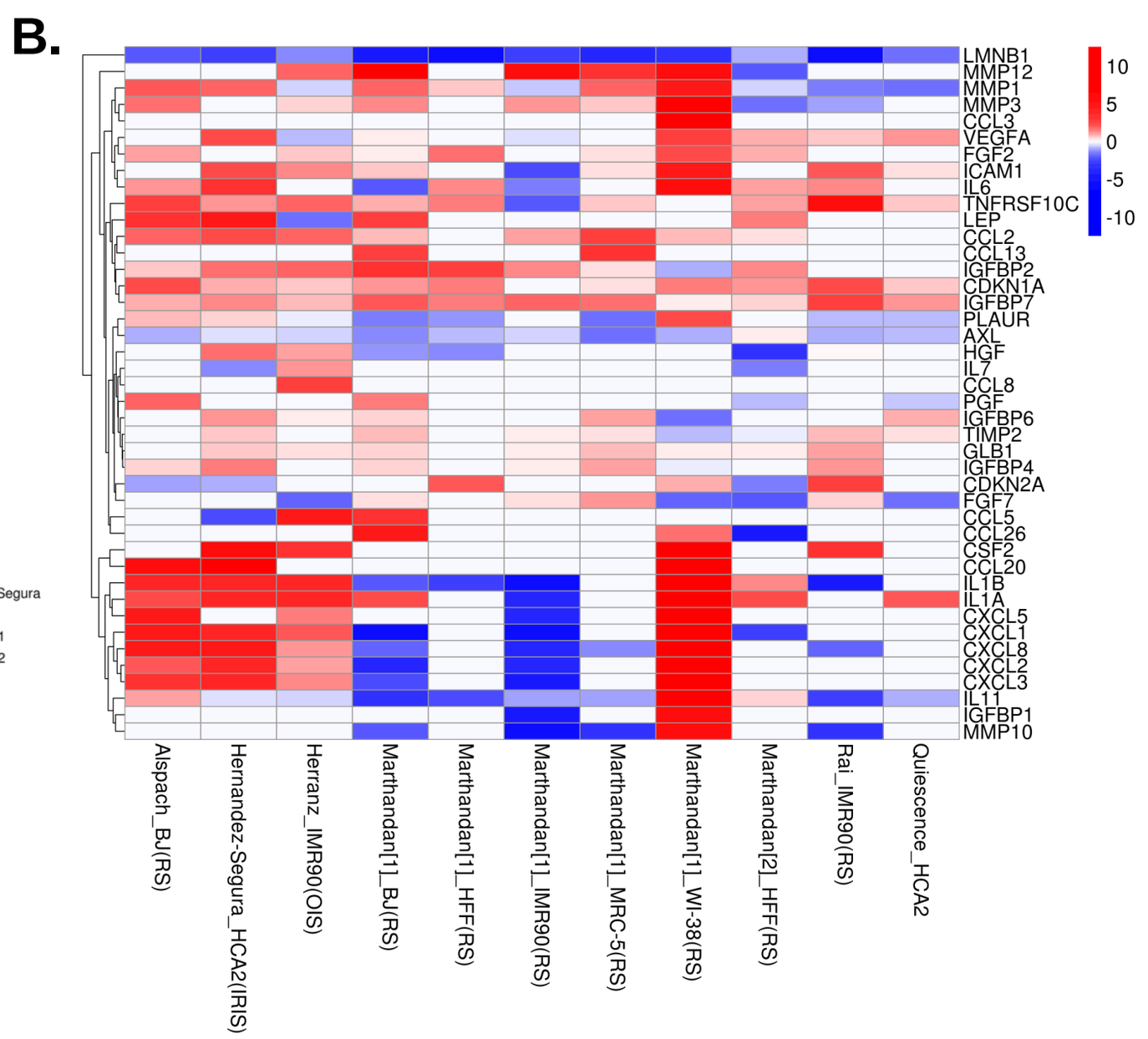

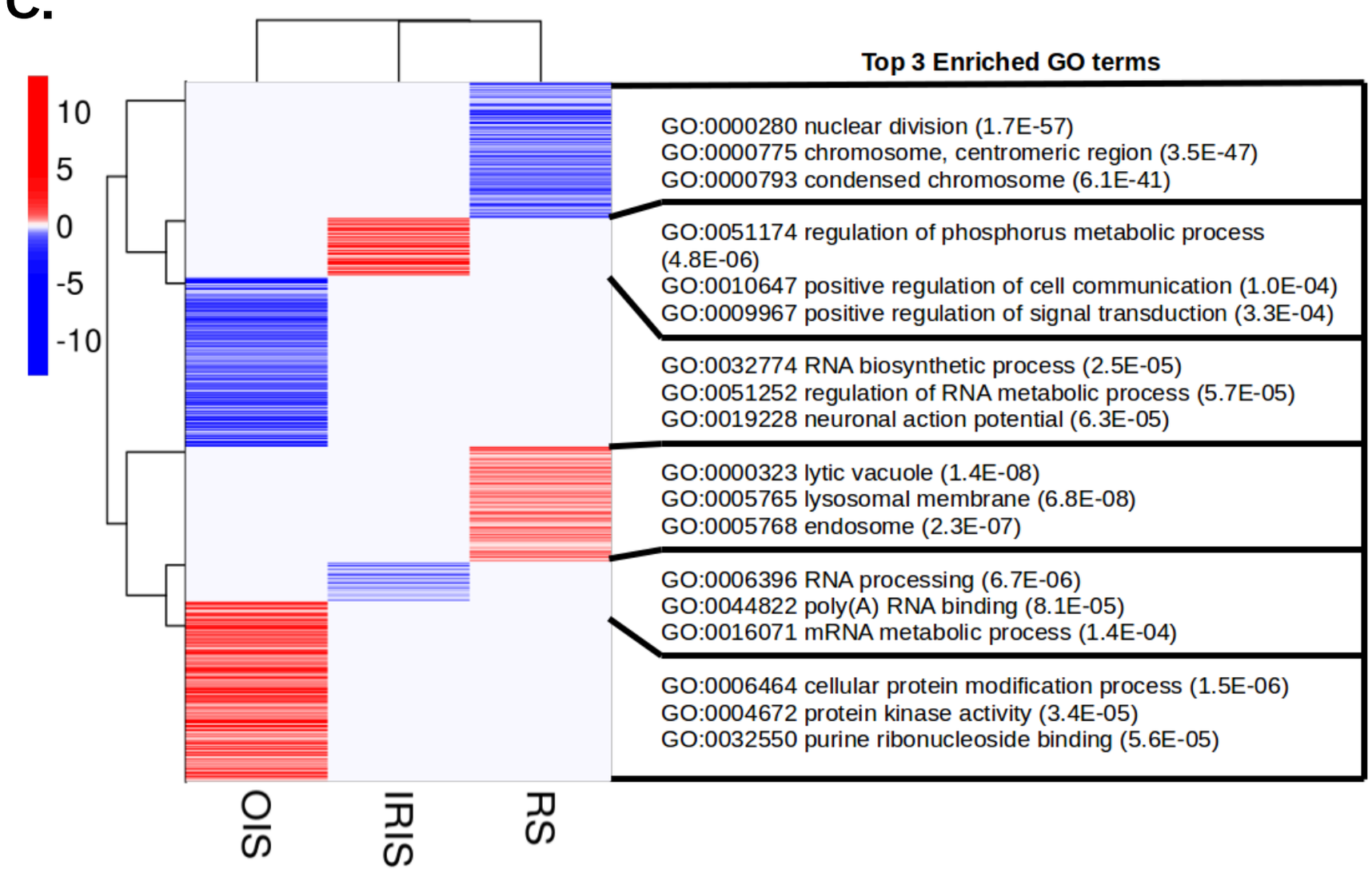

Figure S1. Senescence signatures for fibroblasts.
A. Principal Component Analysis (PCA) of all samples in the selected datasets. The upper panels displays the principal component 2 vs 3 for all the protein-coding genes. The panel on the left upper corner shows each sample colored according to their proliferating or senescence status. The panel on the right upper corner shows each sample colored according to the dataset that they derive from. Samples for each cell type in the same dataset clustered together, with a separation between senescent and proliferating cells from the same dataset. The black arrow shows the only sample (Replicative Senescence in IMR90 cells) that clustered incorrectly. The lower panels display only the genes that were within the Signature of Senescence in Fibroblasts (1311 genes) where it is also evidenced that the same sample clustered differently than its counterparts from the same and other datasets. Based on this evidence, it was decided to remove that sample from further analysis.
B. Heatmap of known senescence markers in all the datasets included in the meta-analysis. The figure shows the logarithm base 2 of the fold change for senescent cells versus proliferating cells of senescence markers: CDKN1A (p21), CDKN2A (p16), GLB1 (beta-gal) and known members of the SASP. Samples are named according to the name of the first author of the dataset, followed by an underscore and the strain of fibroblast depicted in each column. The stimulus used in each dataset is in parentheses: Replicative Senescence (RS), Ionizing Radiation-Induced Senescence (IRIS) and Oncogene-Induced Senescence (OIS).
C. Heatmap of genes that were differentially expressed exclusively by one of the stimuli tested and the corresponding GO terms. The figure shows the logarithm base 2 of the fold change for RS, IRIS and OIS versus proliferating cells. The right side of the panel shows the top 3 enriched GO terms for each stimulus and either up- (red) or down-(blue) regulated genes.

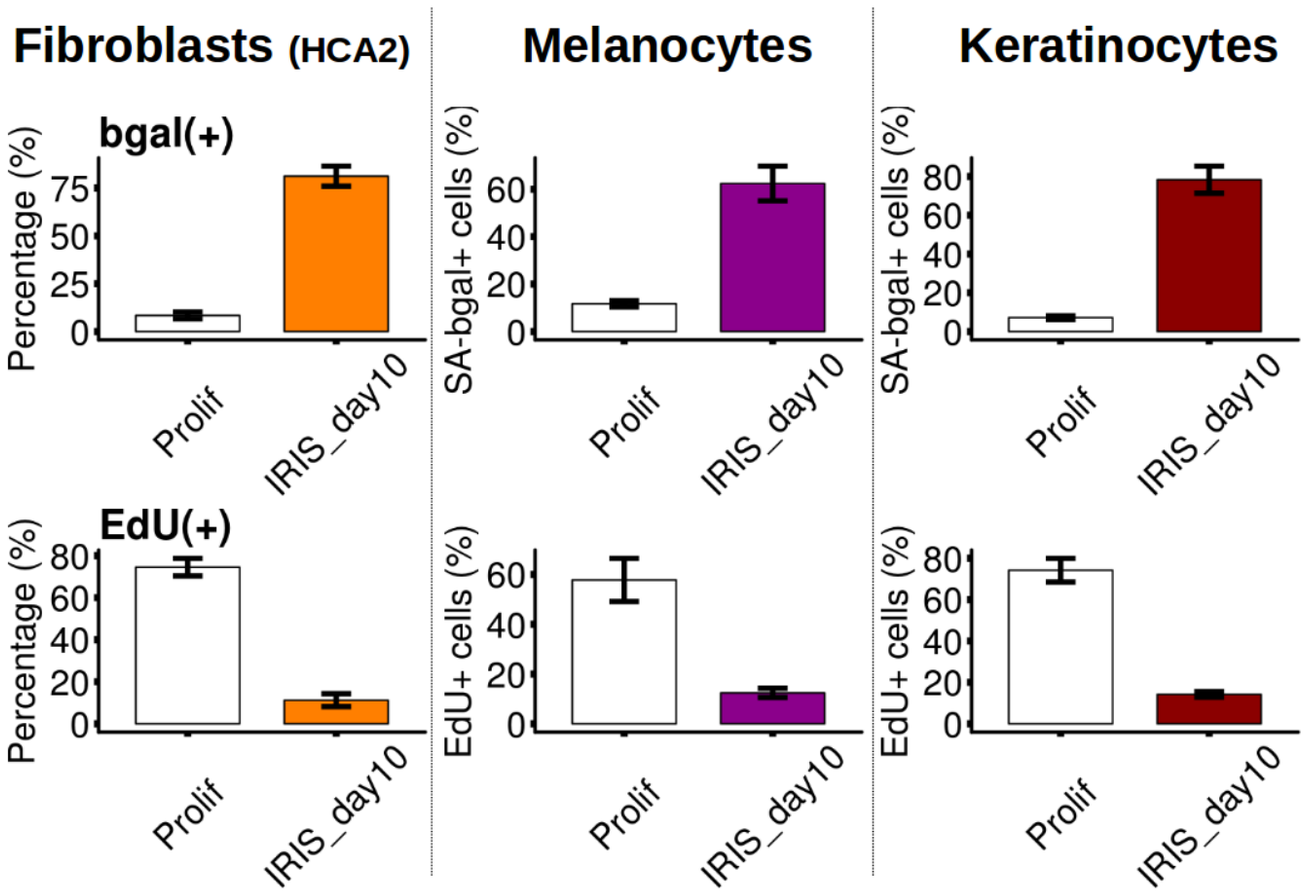

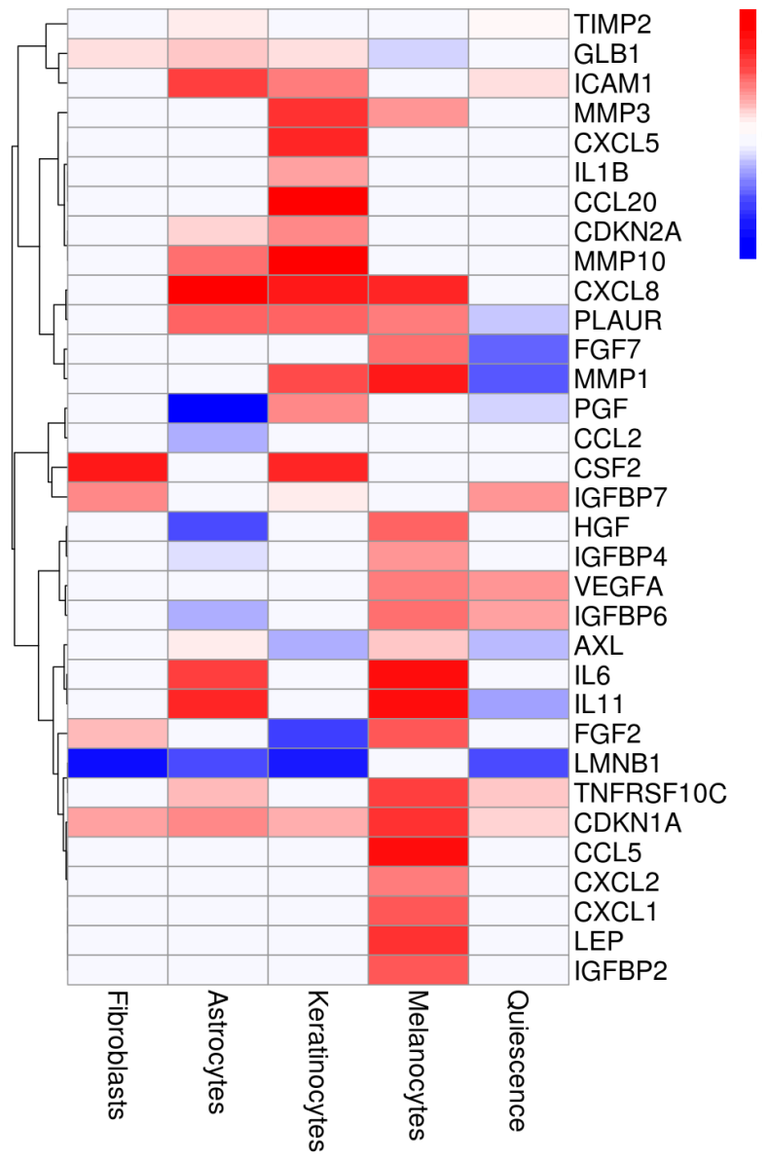

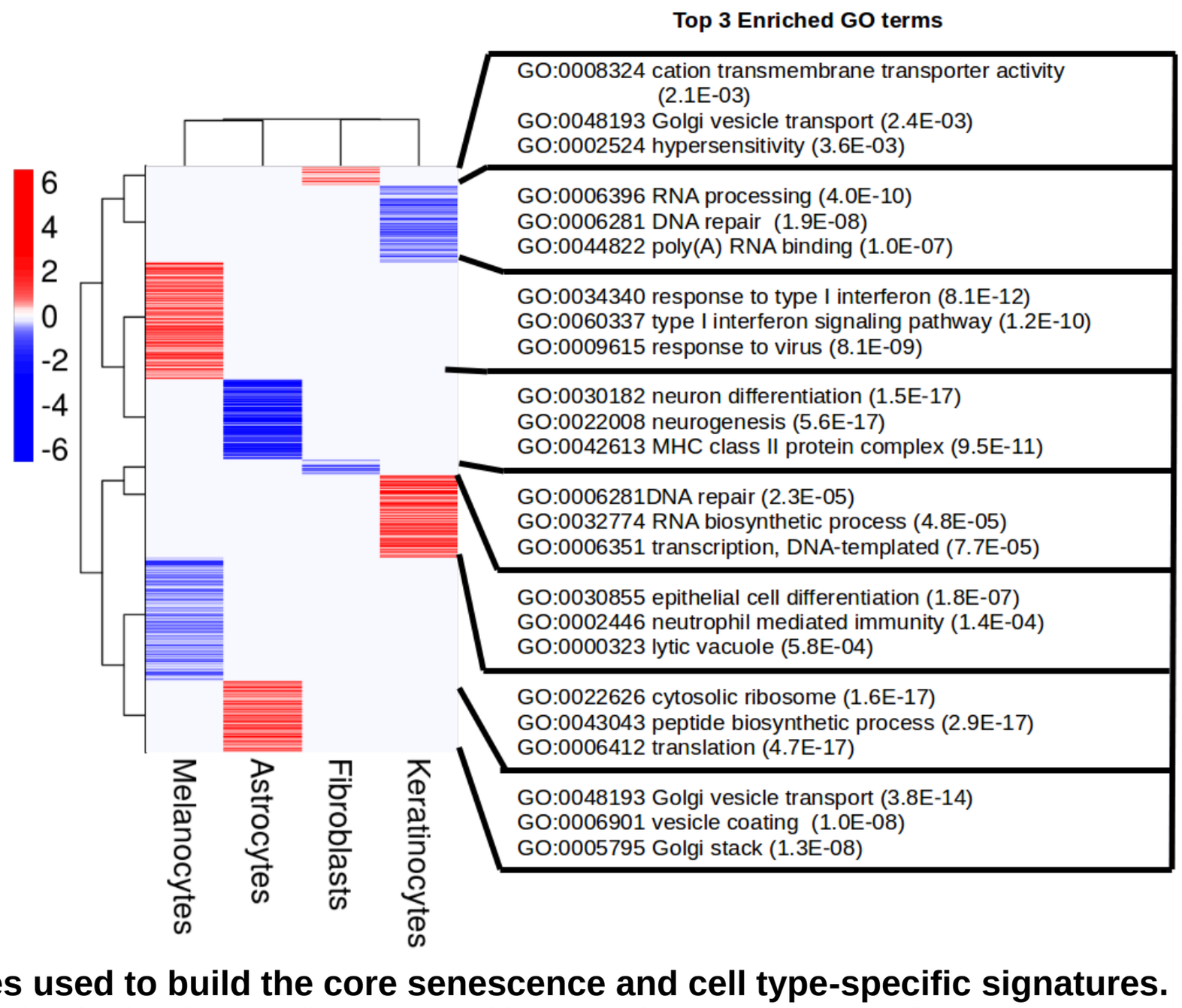

Figure S2. Cell types used to build the core senescence and cell type-specific signatures.
A. Senescence-induction in the three cell types used by our laboratory was confirmed by senescence-associated b-galactosidase (SA-bgal) activity and incorporation of EdU into DNA of proliferating cells. The percentage of positive cells for senescent fibroblasts (yellow), melanocytes (magenta) and keratinocytes (red) and their proliferating counterparts (white) are shown, demonstrating increased SA-Bgal activity and decreased EdU incorporation (proliferation) in senescent cells (10 days post-irradiation).
B. Heatmap of genes that were differentially expressed exclusively in one cell type and the corresponding GO terms. The figure shows the logarithm base 2 of the fold change for senescent fibroblasts, melanocytes, keratinocytes and astrocytes versus their proliferating counterparts. The right side of the panel shows the top 3 enriched GO terms for each stimulus and either up- (red) or down-(blue) regulated genes.
C. Heatmap of known senescence markers in the different Senescent cell types tested and in the Quiescence dataset. The figure shows the logarithm base 2 of the fold change for senescent cells versus proliferating cells of senescence markers: CDKN1A (p21), CDKN2A (p16), GLB1 (SA-bgal) and known members of the SASP. The Fibroblasts refers to the Differentially Expressed Genes in Senescent Fibroblasts product of the meta-analysis (before extracting genes similarly regulated in Quiescence). Melanocytes and Keratinocytes were induced to Senescence with IRIS and Astrocytes with OSIS. Quiescence refers to the sample of HCA2 fibroblasts that was induced to quiescence by serum starvation.

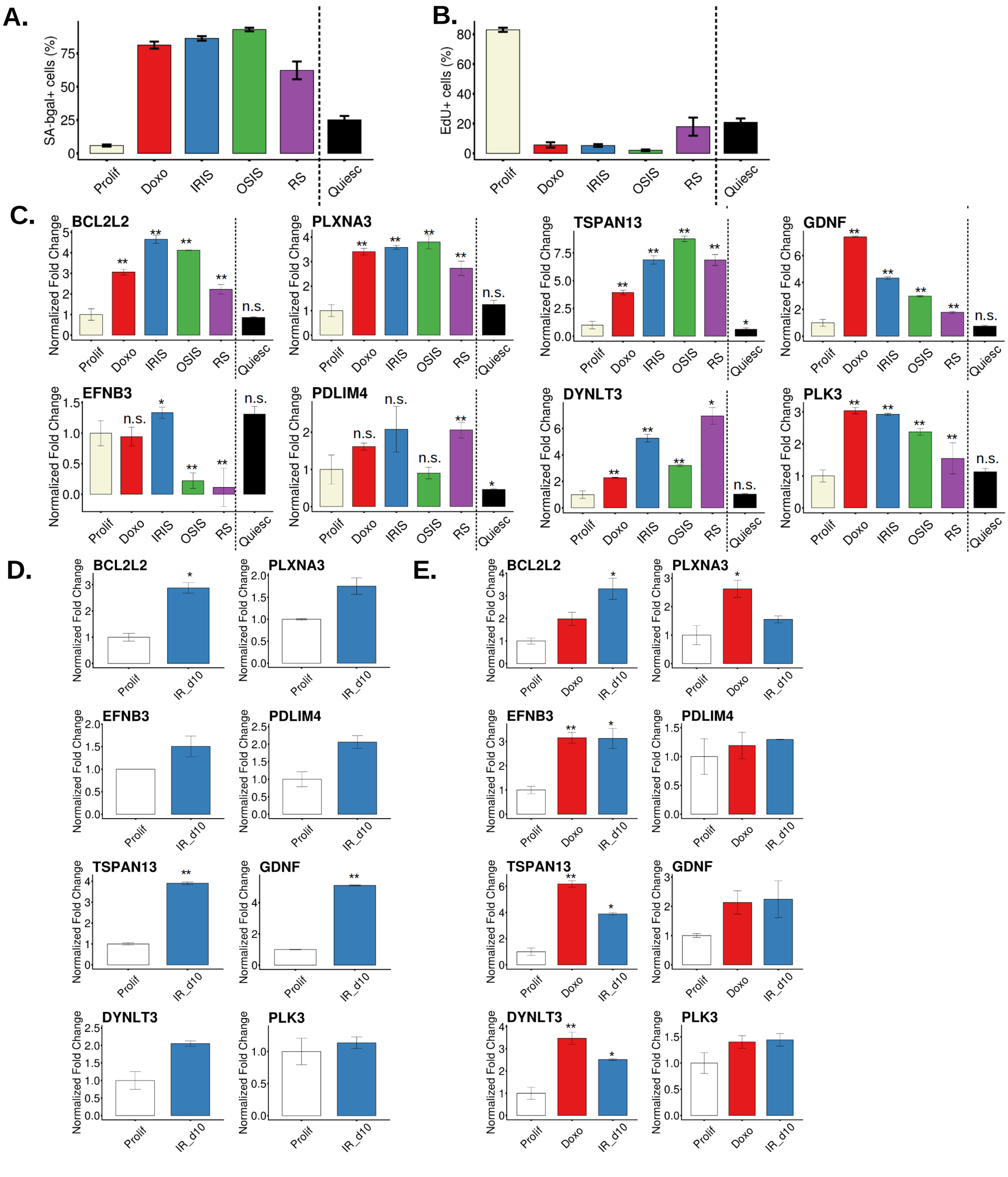

Figure S3. Validation of the core senescence signature.
A-C. Different senescence-inducing stimuli were applied to BJ cells: doxorubicin (red), IRIS (blue), OSIS (green) and RS (violet). Signatures were compared to proliferating (white) and quiescent (black) cells.
A. Percentage of SA-βgal+ cells in proliferating and senescent populations.
B. Percentage of EdUl+ cells in proliferating and senescent populations.
C. Eight genes in the core signature of senescence were validated by Real Time-PCR: BCL2L2, PLXNA3, EFNB3, PDLIM4, TSPAN13, GDNF, DYNLT3 and PLK3. The expression of tubulin was used to normalize the fold changes.
D-E. The above eight genes in the core signature of senescence that were validated in BJ cells (human) were measured in mouse cells. All the genes tested (BCL2L2, PLXNA3, PDLIM4, TSPAN13, GDNF, DYNLT3 and PLK3) followed the same trend, with the exception of EFNB3, which showed an opposite trend. The expression of tubulin was used to normalize the fold changes.
D. Validation of the eight core senescence signature genes in mouse endothelial cells.
E. Validation of the eight core senescence signature genes in mouse embryonic fibroblasts (MEFs).
All samples included two or three biological and two technical replicates. Statistical significance was determined by an unpaired two-tailed Student's t-test on delta-CT values (* = p<=0.05, ** = p<=0.01 and n.s.=not significant).

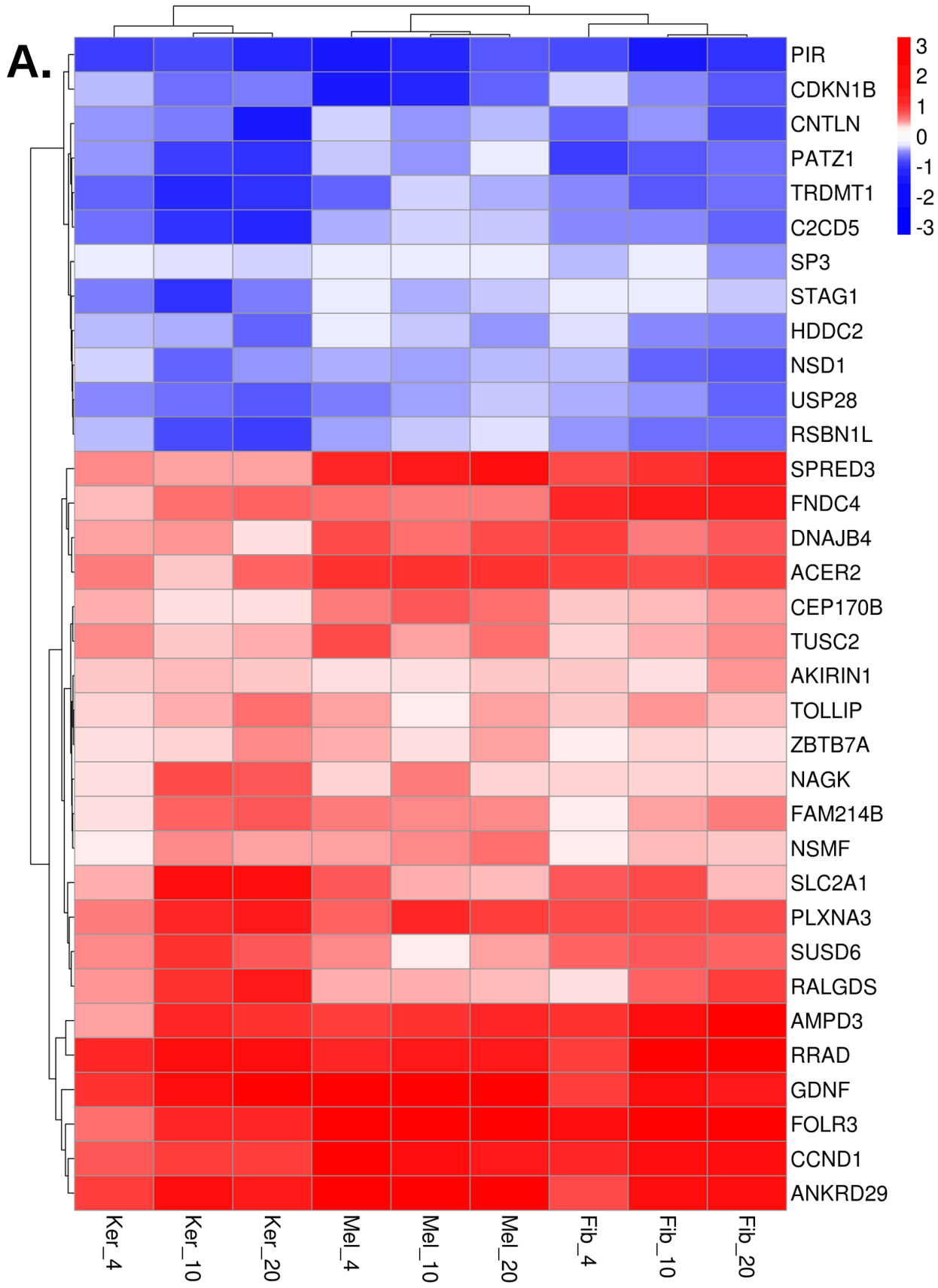

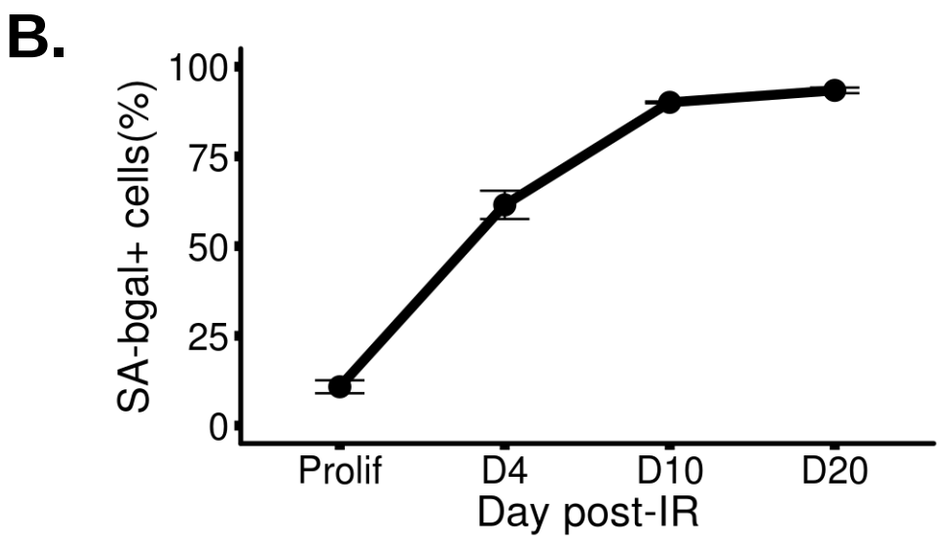

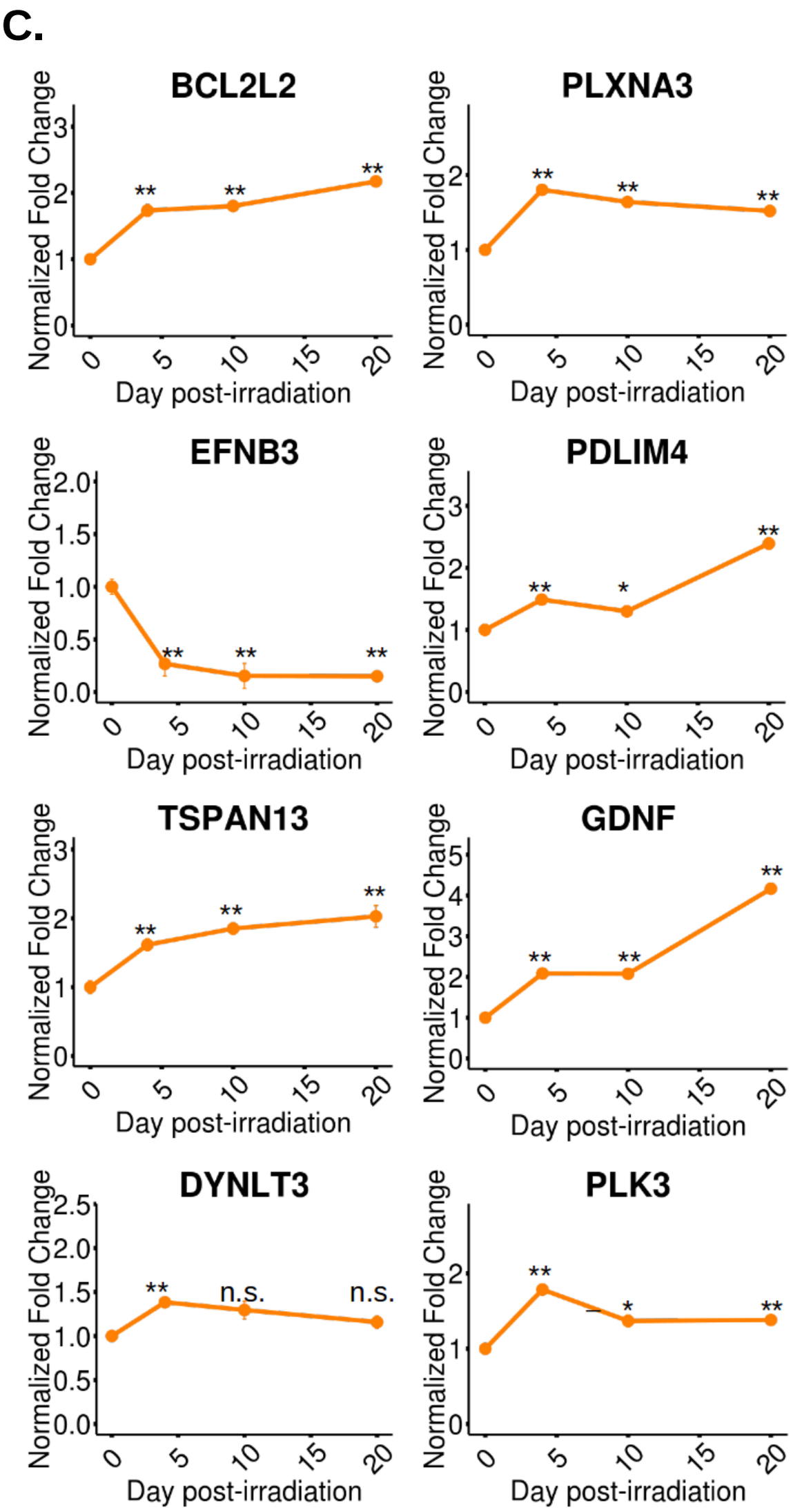

Figure S4. Heatmap of genes shared among different time points and cell types after senescence-induction by ionizing radiation and validation of the temporal dynamics of the core senescence signature.
A. Heatmap of the genes comprising the shared IRIS signature among all time-points and cell types. The heatmap shows the logarithm base 2 of the fold change for each time point (days 4, 10 and 20 post-irradiation) and for each cell type (Fib=fibroblasts, Mel=melanocytes and Ker=keratinocytes) with respect to their proliferating counterparts.
B. Percentage of SA-βgal+ BJ cells at day 0 (proliferation) and days 4, 10 and 20 post-irradiation demonstrating an increase in SA-βgal activity upon irradiation.
C. The eight genes in the core signature of senescence that were validated by Real Time-PCR in BJ cells were confirmed in HCA-2 cells. The temporal dynamics of the genes are demonstrated by the expression trends and lack of statistical significance at some of the time points. The expression of tubulin was used to normalize the fold changes. All samples included three biological and two technical replicates. Statistical significance was determined by an unpaired two-tailed Student's t-test on delta-CT values (* = p<=0.05, ** = p<=0.01 and n.s.=not significant).

Table S1. List of primers for qPCR. Related to STAR methods

Gene	Species	Direction	Sequence	UPL probe
TUBA	Human	FW	cttcgtctccgccatcag	40
		RV	cgtgttccaggcagtagagc	
CDKN2A	Human	FW	gagcagcatggagccttc	67
		RV	cgtaactattcggtgcgttg	
CDKN1A	Human	FW	tcactgtcttgtacccttgtgc	32
		RV	ggcgtttggagtggtagaaa	
IL6	Human	FW	caggagcccagctatgaact	45
		RV	gaaggcagcaggcaacac	
PDLIM4	Human	FW	ggatccacatcgatcctgag	40
		RV	gcttggtctgccatcttctg	
GDNF_v1	Human	FW	atgtccaacctagggtctgc	70
		RV	catcccataacttcatcttaaagtcc	
TSPAN13	Human	FW	tcaacctgctttacaccttgg	84
		RV	aatcagcccgaagccaat	
DYNLT3	Human	FW	gtgctctaccggcgtgtc	25
		RV	cagcattgaagccaacctc	
EFNB3	Human	FW	tggaactcggcgaataagag	13
		RV	cgatctgagggtacagcaca	
PLK3	Human	FW	gaaggtgggggattttgg	6
		RV	gggtgccacagatggtct	
PLXNA3	Human	FW	gagggcactctggctctg	17
		RV	cagaagttgccgttgatctg	
BCL2L2	Human	FW	tggatggtggcctacctg	28
		RV	cgtccccgtatagagctgtg	
TUBA	Mouse	FW	ctggaacccacggtcatc	89
		RV	gtggccacgagcatagttatt	
CDKN2a	Mouse	FW	aatctccgcgaggaaagc	91
		RV	gtctgcagcggactccat	
CDKN1A	Mouse	FW	aacatctcagggccgaaa	16
		RV	tgcgcttggagtgatagaaa	
IL6	Mouse	FW	gctaccaaactggatataatcagga	6
		RV	ccaggtagctatggtactccagaa	
PDLIM4	Mouse	FW	tccacattgaccctgagtcc	40
		RV	cctccagactaatcccagagac	
GDNF	Mouse	FW	tccaactgggggtctacg	70
		RV	gacatcccataacttcatcttagagtc	
TSPAN13	Mouse	FW	gcccccataatcggagag	67
		RV	agccaaacacccaggatct	
DYNLT3	Mouse	FW	actggggaaagcttacaagtaca	82
		RV	ggctgtgtgaaatccatacg	
EFNB3	Mouse	FW	tggaactcggcgaataagag	13
		RV	ccccgatctgaggataaagc	
PLK3_v1_v2	Mouse	FW	ggctggcagctcgattag	6
		RV	gttgggagtgccacagatg	
PLXNA3	Mouse	FW	gagtcagtcgcggtggag	7
		RV	aggcaccctcctatggtga	
BCL2L2	Mouse	FW	agtgcaggattggatggtg	80
		RV	cccgtatagagctgtgaactcc	

Supplemental References list

S1. Abdelmohsen, K., Panda, A., Kang, M.J., Xu, J., Selimyan, R., Yoon, J.H., Martindale, J.L., De, S., Wood, W.H., Becker, K.G., et al. (2013). Senescence-associated lncRNAs: Senescence-associated long noncoding RNAs. Aging Cell *12*, 890-900.

S2. Alspach, E., Flanagan, K.C., Luo, X., Ruhland, M.K., Huang, H., Pazolli, E., Donlin, M.J., Marsh, T., Piwnica-Worms, D., Monahan, J., et al. (2014). P38MAPK plays a crucial role in stromal-mediated tumorigenesis. Cancer Discovery *4*, 716-729.

S3. Capell, B.C., Drake, A.M., Zhu, J., Shah, P.P., Dou, Z., Dorsey, J., Simola, D.F., Donahue, G., Sammons, M., Rai, T.S., et al. (2016). MLL1 is essential for the senescence-associated secretory phenotype. Genes & Development *30*, 321-336.

S4. Dikovskaya, D., Cole, J.J., Mason, S.M., Nixon, C., Karim, S.A., McGarry, L., Clark, W., Hewitt, R.N., Sammons, M.A., Zhu, J., et al. (2015). Mitotic Stress Is an Integral Part of the Oncogene-Induced Senescence Program that Promotes Multinucleation and Cell Cycle Arrest. Cell Reports *12*, 1483-1496.

S5. Duarte, L.F., Young, A.R.J., Wang, Z., Wu, H.-A., Panda, T., Kou, Y., Kapoor, A., Hasson, D., Mills, N.R., Ma'ayan, A., et al. (2014). Histone H3.3 and its proteolytically processed form drive a cellular senescence programme. Nature communications *5*, 5210.

S6. Herranz, N., Gallage, S., Mellone, M., Wuestefeld, T., Klotz, S., Hanley, C.J., Raguz, S., Acosta, J.C., Innes, A.J., Banito, A., et al. (2015). mTOR regulates MAPKAPK2 translation to control the senescence-associated secretory phenotype. Nature cell biology *17*, 1205-1217.

S7. Loayza-Puch, F., Drost, J., Rooijers, K., Lopes, R., Elkon, R., and Agami, R. (2013). p53 induces transcriptional and translational programs to suppress cell proliferation and growth. Genome Biol *14*, R32.

S8. Marthandan, S., Baumgart, M., Priebe, S., Groth, M., Schaer, J., Kaether, C., Guthke, R., Cellerino, A., Platzer, M., Diekmann, S., et al. (2016). Conserved Senescence Associated Genes and Pathways in Primary Human Fibroblasts Detected by RNA-Seq. Plos One *11*, e0154531.

S9. Marthandan, S., Priebe, S., Baumgart, M., Groth, M., Cellerino, A., Guthke, R., Hemmerich, P., and Diekmann, S. (2015). Similarities in Gene Expression Profiles during In Vitro Aging of Primary Human Embryonic Lung and Foreskin Fibroblasts. BioMed research international *2015*, 731938.

S10. Correia-Melo, C., Marques, F.D., Anderson, R., Hewitt, G., Hewitt, R., Cole, J., Carroll, B.M., Miwa, S., Birch, J., Merz, A., et al. (2016). Mitochondria are required for pro-ageing features of the senescent phenotype. The EMBO Journal, e201592862.

S11. Procopio, M.G., Laszlo, C., Al Labban, D., Kim, D.E., Bordignon, P., Jo, S.H., Goruppi, S., Menietti, E., Ostano, P., Ala, U., et al. (2015). Combined CSL and p53 downregulation promotes cancer-associated fibroblast activation. Nat Cell Biol *17*, 1193-1204.

S12. Purcell, M., Kruger, A., and Tainsky, M.A. (2014). Gene expression profiling of replicative and induced senescence. Cell Cycle *13*, 3927-3937.

S13. Rai, T.S., Cole, J.J., Nelson, D.M., Dikovskaya, D., Faller, W.J., Vizioli, M.G., Hewitt, R.N., Anannya, O., McBryan, T., Manoharan, I., et al. (2014). HIRA orchestrates a dynamic chromatin landscape in senescence and is required for suppression of Neoplasia. Genes and Development *28*, 2712-2725.

S14. Crowe, E.P., Tuzer, F., Gregory, B.D., Donahue, G., Gosai, S.J., Cohen, J., Leung, Y.Y., Yetkin, E., Nativio, R., Wang, L.-S., et al. (2016). Changes in the Transcriptome of Human Astrocytes Accompanying Oxidative Stress-Induced Senescence. Frontiers in Aging Neuroscience *8*, 1-13.

S15. Hänzelmann, S., Beier, F., Gusmao, E.G., Koch, C.M., Hummel, S., Charapitsa, I., Joussen, S., Benes, V., Brümmendorf, T.H., Reid, G., et al. (2015). Replicative senescence is associated with nuclear reorganization and with DNA methylation at specific transcription factor binding sites. Clinical epigenetics *7*, 19.

S16. Pawlikowski, J.S., McBryan, T., van Tuyn, J., Drotar, M.E., Hewitt, R.N., Maier, A.B., King, A., Blyth, K., Wu, H., and Adams, P.D. (2013). Wnt signaling potentiates nevogenesis. Proceedings of the National Academy of Sciences of the United States of America *110*, 16009-16014.

S17. Lee, J.H., Zhao, X.M., Yoon, I., Lee, J.Y., Kwon, N.H., Wang, Y.Y., Lee, K.M., Lee, M.J., Kim, J., Moon, H.G., et al. (2016). Integrative analysis of mutational and transcriptional profiles reveals driver mutations of metastatic breast cancers. Cell Discov *2*, 16025.

S18. Notsuda, H., Sakurada, A., Endo, C., Okada, Y., Horii, A., Shima, H., and Kondo, T. (2013). p190A RhoGAP is involved in EGFR pathways and promotes proliferation, invasion and migration in lung adenocarcinoma cells. Int J Oncol *43*, 1569-1577.

S19. Li, M., Zhao, H., Zhang, X., Wood, L.D., Anders, R.A., Choti, M.A., Pawlik, T.M., Daniel, H.D., Kannangai, R., Offerhaus, G.J., et al. (2011). Inactivating mutations of the chromatin remodeling gene ARID2 in hepatocellular carcinoma. Nat Genet *43*, 828-829.

S20. Manceau, G., Letouze, E., Guichard, C., Didelot, A., Cazes, A., Corte, H., Fabre, E., Pallier, K., Imbeaud, S., Le Pimpec-Barthes, F., et al. (2013). Recurrent inactivating mutations of ARID2 in non-small cell lung carcinoma. Int J Cancer *132*, 2217-2221.

S21. Yosef, R., Pilpel, N., Tokarsky-Amiel, R., Biran, A., Ovadya, Y., Cohen, S., Vadai, E., Dassa, L., Shahar, E., Condiotti, R., et al. (2016). Directed elimination of senescent cells by inhibition of BCL-W and BCL-XL. Nature communications *7*, 11190.

S22. Wang, H.R., Xiao, Z.Y., Chen, M., Wang, F.L., Liu, J., Zhong, H., Zhong, J.H., Ou-Yang, R.R., Shen, Y.L., and Pan, S.M. (2012). Anti-CHMP5 single chain variable fragment antibody retrovirus infection induces programmed cell death of AML leukemic cells in vitro. Acta Pharmacol Sin *33*, 809-816.

S23. Bandyopadhyay, D., Okan, N.a., and Bales, E. (2002). Down-Regulation of p300 / CBP Histone Acetyltransferase Activates a Senescence Checkpoint in Human Melanocytes Down-Regulation of p300 / CBP Histone Acetyltransferase Activates a Senescence. Cell, 6231-6239.

S24. Zhang, M., Poplawski, M., Yen, K., Cheng, H., Bloss, E., Zhu, X., Patel, H., and Mobbs, C.V. (2009). Role of CBP and SATB-1 in aging, dietary restriction, and insulin-like signaling. PLoS Biol *7*, e1000245.

S25. Cheng, L., Yang, Q., Li, C., Dai, L., Yang, Y., Wang, Q., Ding, Y., Zhang, J., Liu, L., Zhang, S., et al. (2017). DDA1, a novel oncogene, promotes lung cancer progression through regulation of cell cycle. J Cell Mol Med.

S26. Chen, S.S., Hu, Z., and Zhong, X.P. (2016). Diacylglycerol Kinases in T Cell Tolerance and Effector Function. Front Cell Dev Biol *4*, 130.

S27. Lo, K.W., Kogoy, J.M., and Pfister, K.K. (2007). The DYNLT3 light chain directly links cytoplasmic dynein to a spindle checkpoint protein, Bub3. J Biol Chem *282*, 11205-11212.

S28. Ståhl, S., Kaminskyy, V.O., Efazat, G., Hyrslova Vaculova, a., Rodriguez-Nieto, S., Moshfegh, a., Lewensohn, R., Viktorsson, K., and Zhivotovsky, B. (2013). Inhibition of Ephrin B3-mediated survival signaling contributes to increased cell death response of non-small cell lung carcinoma cells after combined treatment with ionizing radiation and PKC 412. Cell death & disease *4*, e454.

S29. Hansford, L.M., and Marshall, G.M. (2005). Glial cell line-derived neurotrophic factor (GDNF) family ligands reduce the sensitivity of neuroblastoma cells to pharmacologically induced cell death, growth arrest and differentiation. Neurosci Lett *389*, 77-82.

S30. Ito, Y., Okada, Y., Sato, M., Sawai, H., Funahashi, H., Murase, T., Hayakawa, T., and Manabe, T. (2005). Expression of glial cell line-derived neurotrophic factor family members and their receptors in pancreatic cancers. Surgery *138*, 788-794.

S31. Iwahashi, N., Nagasaka, T., Tezel, G., Iwashita, T., Asai, N., Murakumo, Y., Kiuchi, K., Sakata, K., Nimura, Y., and Takahashi, M. (2002). Expression of glial cell line-derived neurotrophic factor correlates with perineural invasion of bile duct carcinoma. Cancer *94*, 167-174.

S32. Wang, Z., Rong, X., Luo, B., Qin, S., Lu, L., Zhang, X., Sun, Y., Hu, Q., and Zhang, C. (2016). A Natural Model of Mouse Cardiac Myocyte Senescence. Journal of Cardiovascular Translational Research, 4-6.

S33. Lee, J.S., Xiao, J., Patel, P., Schade, J., Wang, J., Deneen, B., Erdreich-Epstein, A., and Song, H.R. (2014). A novel tumor-promoting role for nuclear factor IA in glioblastomas is mediated through negative regulation of p53, p21, and PAI1. Neuro Oncol *16*, 191-203.

S34. Stanley, R.F., Piszczatowski, R.T., Bartholdy, B., Mitchell, K., McKimpson, W.M., Narayanagari, S., Walter, D., Todorova, T.I., Hirsch, C., Makishima, H., et al. (2017). A myeloid tumor suppressor role for NOL3. J Exp Med *214*, 753-771.

S35. Gilkes, D.M., Bajpai, S., Chaturvedi, P., Wirtz, D., and Semenza, G.L. (2013). Hypoxia-inducible factor 1 (HIF-1) promotes extracellular matrix remodeling under hypoxic conditions by inducing P4HA1, P4HA2, and PLOD2 expression in fibroblasts. J Biol Chem *288*, 10819-10829.

S36. Cho, J.H., Kim, M.J., Kim, K.J., and Kim, J.R. (2012). POZ/BTB and AT-hook-containing zinc finger protein 1 (PATZ1) inhibits endothelial cell senescence through a p53 dependent pathway. Cell Death Differ *19*, 703-712.

S37. Vanaja, D.K., Ballman, K.V., Morlan, B.W., Cheville, J.C., Neumann, R.M., Lieber, M.M., Tindall, D.J., and Young, C.Y.F. (2006). PDLIM4 repression by hypermethylation as a potential biomarker for prostate cancer. Clinical Cancer Research *12*, 1128-1136.

S38. Vanaja, D.K., Grossmann, M.E., Cheville, J.C., Gazi, M.H., Gong, A., Zhang, J.S., Ajtai, K., Burghardt, T.P., and Young, C.Y.F. (2009). PDLIM4, an actin binding protein, suppresses prostate cancer cell growth. Cancer investigation *27*, 264-272.

S39. Xu, D., Yao, Y., Lu, L., Costa, M., and Dai, W. (2010). Plk3 functions as an essential component of the hypoxia regulatory pathway by direct phosphorylation of HIF-1alpha. J Biol Chem *285*, 38944-38950.

S40. Arakawa, M., Yasutake, M., Miyamoto, M., Takano, T., Asoh, S., and Ohta, S. (2007). Transduction of anti-cell death protein FNK protects isolated rat hearts from myocardial infarction induced by ischemia/reperfusion. Life Sci *80*, 2076-2084.

S41. Hsu, Y.C., Chen, H.Y., Yuan, S., Yu, S.L., Lin, C.H., Wu, G., Yang, P.C., and Li, K.C. (2013). Genome-wide analysis of three-way interplay among gene expression, cancer cell invasion and anti-cancer compound sensitivity. BMC Med *11*, 106.

S42. Cheng, L., Lu, W., Kulkarni, B., Pejovic, T., Yan, X., Chiang, J.H., Hood, L., Odunsi, K., and Lin, B. (2010). Analysis of chemotherapy response programs in ovarian cancers by the next-generation sequencing technologies. Gynecol Oncol *117*, 159-169.

S43. Breslin, L., Prosser, S.L., Cuffe, S., and Morrison, C.G. (2014). Ciliary abnormalities in senescent human fibroblasts impair proliferative capacity. Cell Cycle *13*, 2773-2779.

S44. Polato, F., Rusconi, P., Zangrossi, S., Morelli, F., Boeri, M., Musi, A., Marchini, S., Castiglioni, V., Scanziani, E., Torri, V., et al. (2014). DRAGO (KIAA0247), a new DNA damage-responsive, p53-inducible gene that cooperates with p53 as oncosuppressor. [Corrected]. J Natl Cancer Inst *106*, dju053.

S45. Torun, A., Szymanska, E., Castanon, I., Wolinska-Niziol, L., Bartosik, A., Jastrzebski, K., Mietkowska, M., Gonzalez-Gaitan, M., and Miaczynska, M. (2015). Endocytic Adaptor Protein Tollip Inhibits Canonical Wnt Signaling. PLoS One *10*, e0130818.

S46. Lewinska, A., Wnuk, M., Grabowska, W., Zabek, T., Semik, E., Sikora, E., and Bielak-Zmijewska, A. (2015). Curcumin induces oxidation-dependent cell cycle arrest mediated by SIRT7 inhibition of rDNA transcription in human aortic smooth muscle cells. Toxicol Lett *233*, 227-238.

S47. Huang, H., Sossey-Alaoui, K., Beachy, S.H., and Geradts, J. (2007). The tetraspanin superfamily member NET-6 is a new tumor suppressor gene. Journal of Cancer Research and Clinical Oncology *133*, 761-769.

S48. Arencibia (1992). Gene expression profiling reveals overexpression of TSPAN13 in prostate cancer. International Journal of Oncology.

S49. Vredeveld, L.C., Rowland, B.D., Douma, S., Bernards, R., and Peeper, D.S. (2010). Functional identification of LRF as an oncogene that bypasses RASV12-induced senescence via upregulation of CYCLIN E. Carcinogenesis *31*, 201-207.

S50. Kumari, R., Li, H., Haudenschild, D.R., Fierro, F., Carlson, C.S., Overn, P., Gupta, L., Gupta, K., Nolta, J., Yik, J.H., et al. (2012). The oncogene LRF is a survival factor in chondrosarcoma and contributes to tumor malignancy and drug resistance. Carcinogenesis *33*, 2076-2083.

S51. Wang, G., Lunardi, A., Zhang, J., Chen, Z., Ala, U., Webster, K.A., Tay, Y., Gonzalez-Billalabeitia, E., Egia, A., Shaffer, D.R., et al. (2013). Zbtb7a suppresses prostate cancer through repression of a Sox9-dependent pathway for cellular senescence bypass and tumor invasion. Nat Genet *45*, 739-746.

S52. He, P., Sun, L., Zhu, D., Zhang, H., Zhang, L., Guo, Y., Liu, S., Zhou, J., Xu, X., and Xie, P. (2016). Knock-Down of Endogenous Bornavirus-Like Nucleoprotein 1 Inhibits Cell Growth and Induces Apoptosis in Human Oligodendroglia Cells. Int J Mol Sci *17*, 435.

S53. Lafarga, V., Cuadrado, A., and Nebreda, A.R. (2007). p18(Hamlet) mediates different p53-dependent responses to DNA-damage inducing agents. Cell Cycle *6*, 2319-2322.